Nanozeolites as support for laccase immobilization: Application to mediated glycerol oxidation

Alex Henrique Miller [a,1], Adriano de Vasconcellos [a], Alistair John Fielding [b], José Geraldo Nery [a,*]

[a] Physics Department, Institute of Biosciences, Letters, and Exact Sciences – IBILCE / São Paulo State University – UNESP, São José do Rio Preto, São Paulo, 15054-000, Brazil.

[b] Centre for Natural Products Discovery, School of Pharmacy and Biomolecular Science, Liverpool John Moores University, James Parsons Building, Byrom Street, Liverpool, L3 3AF, United Kingdom.

*Corresponding author: José Geraldo Nery (geraldo.nery@unesp.br)

[1] Present address: Department of Chemistry, University of York, Heslington, York, YO10 5DD, United Kingdom.

Abstract

This study investigated the use of nanozeolites as support for laccases from *P. ostreatus* (LPO), *Aspergillus* sp (LAsp) and *A. bisporus* (LAB) immobilization applied to 2,2,6,6-tetramethylpiperidine-N-oxyl (TEMPO) mediated glycerol oxidation. Selected complexes led to up to 5% glycerol conversion, and interestingly, up to 100% selectivity to glyceraldehyde after 48 h. Free enzymes led to significantly higher yields (up to 82%) but lacked on selectivity when tested under the same conditions. These findings suggest that laccases immobilized into nanozeolites are promising catalysts for the selective oxidation of glycerol. With the aim to understand the different behavior of free or immobilized enzymes, electron paramagnetic resonance (EPR) spectroscopy was applied. A significant shift of the T2 parallel copper hyperfine coupling constant was observed. This suggested a perturbation on the catalytic site after immobilization due to pH variation of the enzymatic microenvironments, thus influencing performance of laccase immobilized on nanozeolites.

Keywords: Nanozeolites. Laccase. Immobilization. Glycerol. Oxidation. EPR.

1. Introduction

Glycerol (1,2,3-propanetriol) (GLY), commonly used as a renewable solvent in many chemical processes [1], has lately been widely studied as a versatile building block. Its highly functionalized structure, containing three hydroxyl groups, enables it to be transformed into a plethora of value-added chemicals [2]. Furthermore, glycerol is the main co-product of biodiesel manufacture. The recent increase in biodiesel production has led to a glycerol market surplus, and the price of glycerol has dropped significantly. Moreover, crude glycerol from transesterification demands costly

purification to make it suitable as feedstock for industrial deployment. This makes the synthesis of value-added products from glycerol a key step for making both, biodiesel manufacture and crude glycerol purification, economically feasible [1, 2].

On the other hand, transforming glycerol into new products highly depends on catalysts and catalytic routes. This has motivated studies in the development of new technologies and routes to transform glycerol and expand its market. Among the transformation routes, oxidation is one that provides glycerol conversion into several value-added products [1], such as glyceraldehyde (GcAd), oxalic acid (OAc), formic acid (FAc), glyoxylic acid (GoAc), glycolic acid (GcAc), mesoxalic acid (MAc), tartronic acid (TAc), 1,3-dihydroxyaceton (DHA), glyceric acid (GAc) and hydroxypyruvic acid (HpAc) with applications in several different areas [3-6]. However, selectively oxidizing glycerol is challenging, as it demands the usage of appropriate catalysts under very specific reaction conditions [7].

The catalytic routes employed for glycerol oxidation vary from heterogeneous or homogeneous catalysis to biocatalysis or electrochemical oxidation [8]. Heterogeneous catalysts use a commonly supported noble metal, with limited reuse and high cost [1, 2, 9]. Homogeneous catalysis is mainly performed using expensive stoichiometric oxidants, such as halogenated organic solvents, and generates hazardous or toxic waste, that reduces their industrial interest [1, 3, 8, 10, 11].

Biocatalysis is an alternative route, where microorganisms and enzymes uses glycerol as a carbon substrate [8]. Special attention is given here to the enzymatic glycerol oxidation performed by the multi-copper containing laccases (EC 1.10.3.2 ρ-diphenol:dioxygen oxidoreductases) in a TEMPO-mediated system [9, 12-14]. Laccase-mediator systems (LMS) are widely used in organic synthesis typically using ABTS,

syringaldazine, β-diketones, and TEMPO as mediator. They are considered a green alternative to established routes using problematic terminal oxidants such as hypochlorite [15-18], however concerning the green oxidation of glycerol in an enzyme-mediator system is still scarce. The laccase from *T. hirsuta* in its free form, or immobilized onto silica pellets, was used for this purpose [12]. A sequential oxidation of glycerol has been observed to glyceraldehyde, glyceric acid, tartronic acid, and finally, to mesoxalic acid. Moreover, it was indicated that the product yield depended on TEMPO concentration, and that free and immobilized enzymes performed differently. Although the free enzyme presented increased formation of products, it lacked stability over time, while the immobilized laccases showed the opposite behavior. Although only a small number of studies have endeavored in this field, the reports have pointed out that the laccase/TEMPO-mediated glycerol oxidation is a promising system for the selective glycerol oxidation. The understanding and development of environment-friendly heterogeneous biocatalysts for the selective glycerol oxidation would certainly lead to glycerol and, concomitantly, biodiesel, economic appreciation.

The search for an appropriate support is key for any enzyme immobilization, and it lies on how well the support can retain enzyme activity, stability and reusability. The application of laccases is wide, and several reports describe the immobilization of this enzyme on organic and inorganic supports [19]. In previous studies, we reported the use of nanozeolites as supports for lipases immobilization and the complexes application for biodiesel production [20, 21]. The modulation of these inorganic supports allowed a broad search for supports that not only retained enzyme activity, but improved it, alongside good stability and reusability. The reduction of the size of zeolite particles to

the nanometer scale can lead to significant changes in their physicochemical properties, such as increasing their external area, allowing better access to and exposure of their active sites, high dispersibility in both aqueous and organic solutions and easy adjustment of their tunable surface properties, especially regarding the surface charge and hydrophilicity/hydrophobicity properties [22]. The use of lipases-microzeolites and lipase-nanozeolites complexes in the production of biodiesel has led to the conclusion that lipases-nanozeolites complexes are more efficient catalysts in the production of fatty acid ethyl esters (FAEEs) [21].

To the best of our knowledge, only alumina pellets and Na-alginate matrixes have been employed to laccases immobilization and complexes applied to glycerol TEMPO-mediated oxidation [9, 12, 13]. This gave rise to the following questions: a) Would it be possible to take advantage of the physicochemical properties of nanozeolites to immobilize laccases? b) What would be the catalytic performance of the nanozeolite-lacases complexes in the TEMPO-mediated glycerol oxidation in comparison with the free enzymes? c) Would the support/enzyme interaction lead to any structural perturbation of the catalytic site, and so reflect on changes on catalytic activity? In order to properly answer these questions systematic experiments involving nanozeolites syntheses and their use as solid supports for the immobilization of laccases from *P. ostreatus* (LPO), *Aspergillus* sp (LAsp) and *A. bisporus* (LAB). Afterwards the nanozeolite-enzymes complexes were used as biocatalysts for glycerol oxidation using TEMPO as mediator. Although there are a plethora of laccases enzymes which in principle can be used for the green oxidation of glycerol only T. hirsuta or T. versicolor have been so far investigated, therefore in this study the potential of *Pleurotus*

ostreatus, *Agaricus bisporus* and *Aspergillus* sp laccases are for the first time investigated aiming the green glycerol oxidation.

2. Materials and methods

2.1. Materials

All reagents used in this study, including enzymes, were acquired from Sigma-Aldrich. Inorganic salts and organic bases were used for the preparation of nanozeolitic matrices, as well as organic compounds used in the chemical functionalization of these materials were of reagent grade (≥98%). The enzymes studied were the laccases (EC 1.10.3.2) from *Pleurotus ostreatus*, *Agaricus bisporus* and *Aspergillus* sp. Glycerol (>99%), 2,2,6,6-tetramethylpiperidine-N-oxil (TEMPO) (98%) and 2,2'-azino-bis (3-ethylbenzothiazolin-6-sulphonic acid) (ABTS) (≥98%). Acids, solvents and standards used for HPLC analyses were of HPLC grade (≥99%). All reagents were used as acquired, except the laccase from *Aspergillus* sp, which in some cases underwent filtering and/or buffer exchange processes, using Amicon® Ultra-0.5 (Ultracel-10 membrane, 10 kDa). LAsp is referred as "**untreated**" or "**treated**" when used without filtering or filtered, respectively. The free treated and untreated were tested for glycerol oxidation, and results were statistically the same.

2.2. Preparation of the nanozeolitic supports

The synthesis of the faujasite type X (FAU/Na^+), titanium silicalite (TS-1), zeolite socony mobil-5 (ZSM-5), linde type A (LTA) and beta (BEA) nanozeolites were carried out according to previous described methods: FAU/Na^+ [23, 24], TS-1 [25, 26], ZSM-5 [27], LTA [28] and BEA [29]. The FAU/Na^+ nanozeolite was submitted to an ion exchange process to replace sodium cations for copper dications, similarly to previously

reported [20]. 1 g of FAU/Na^+ was suspended in 30 mL 0.5 M $CuSO_4$ water solution in a 50 mL flask, sealed, magnetically stirred (1200 rpm) at room temperature for 1 h, and then incubated at 80 °C for 7 days under static conditions. Then, the product was centrifuged for 5 minutes (13,000 x *g*), washed several times, and dried at 60 °C overnight. The ion exchanged derivative was designated FAU/Cu^{2+}. Ion exchange experiments were performed only for FAU/Na^+ since the other nanozeolites have low aluminum content which precludes ion exchange with extra framework cations.

2.3. Functionalization and cross-linking of the nanozeolitic supports

The alkoxysilane functionalization using (3-aminopropyl)trimethoxysilane (APTMS) and cross-linking using glutaraldehyde (GA) were performed following the procedure previously described [21]. Prior to the functionalization, the as-synthesized nanozeolites TS-1, ZSM-5, LTA, and BEA were calcinated. The samples were heated in an air stream at 550 °C, using temperature ramps [21]. The FAU/Na^+ and FAU/Cu^{2+} supports were not treated as no template was used in their synthesis. The alkoxysilane functionalized nanozeolites obtained were denoted FAU/Na^+/APTMS, FAU/Cu^{2+}/APTMS, TS-1/APTMS, ZSM-5/APTMS, LTA/APTMS and BEA/APTMS. The cross-linked materials were named FAU/Na^+/APTMS/GA, FAU/Cu^{2+}/APTMS/GA, TS-1/APTMS/GA, ZSM-5/APTMS/GA, LTA/APTMS/GA and BEA/APTMS/GA.

2.4. Physicochemical characterization of supports and supports-enzymes complexes

The prepared materials described above were characterized using X-ray diffraction (XRD), scanning electron microscopy (SEM) and transmission electron microscopy (TEM). The XRD analyses were performed with a MiniFlex II instrument (Rigaku, Tokyo, Japan) equipped with a rotating anode source with flat-plate Bragg-Brentano

geometry and a graphite monochromator, operating at 40 kV and 40 mA, with Cu K_α radiation (wavelength = 1.5418 Å). The powder diffraction patterns were recorded in the 2θ range from 3 to 50 °, with scanning at a goniometer rate of 2° min^{-1}. SEM images were recorded using a 400-L FEI (FEI/Magellan) instrument, coupled with energy dispersive X-ray analyzer, and the sample grid was observed at 5 kV. A thin coating of gold was deposited onto the samples prior to the SEM analyses. TEM data were obtained from powdered glasses suspended in isopropanol and deposited on grids using a FEI TECNAI G2 F20 HRTEM (200 kV) microscope equipped with a field emission gun. Fourier transform infrared (FTIR) spectra were acquired using a PerkinElmer Frontier FTIR spectrometer equipped with an Attenuated Total Reflectance (ATR) accessory. The samples were scanned 64 times between 4000 and 400 cm^{-1}, at a resolution of 4 cm^{-1}.

The continuous wave electron paramagnetic resonance (CW EPR) measurements were performed on a X-band (9.4 GHz) EMXmicro BRUKER spectrometer at 20 K (temperature control by Oxford Instruments CF935 cryostat) using 100 kHz modulation frequency and 0.8 mT modulation amplitude. The microwave power used was 0.27 mW. Field calibration was carried out using 2,2-diphenyl-1-picrylhydrazyl. The spectra were recorded as, solid, frozen solids and exhibit a random collection of orientations of the paramagnetic centers with respect to the applied magnetic field. The corresponding anisotropic *g* and *A* tensors extracted from the spectra provide information about the magnetic environment of the copper centers. The simulations of the CW EPR spectra were performed using the Easyspin simulation software package [30]. Some zeolites have shown low levels of metallic impurities (either Fe^{3+} or Cu^{2+}) possibly arising from the calcination step.

2.5. Laccases immobilization onto cross-linked zeolites

The commercial laccases LPO, LAB and LAsp were covalently immobilized onto the APTMS/GA modified nanozeolites. Initially, stock solutions of the solid extract laccases LPO and LAB (0.5 mg/mL) were prepared in 100 mM acetate buffer (pH 5), and stored at 8 °C until use. The LAsp laccase, purchased already in solution, was diluted in acetate buffer to the concentration of 0.5 mg/mL. The immobilization protocol consisted of suspending 1 g of APTMS/GA modified nanozeolite in 15 mL of laccase solution, magnetically stirring for 16 h at room temperature, followed by separation by centrifugation (11,000 x *g*). The supernatant was stored for remaining activity and protein loading measurements. The precipitate was washed with acetate buffer (100 mM, pH 5) 5x, dried at room temperature, and then stored at 8 °C until use. The amount of the immobilized enzymes adsorbed on the zeolitic matrixes, was determined according to the method described by Bradford [31].

2.6. Determination of enzymatic activities

The free or immobilized laccase activities were determined according to the study of Liebminger et al. (2009)[12]. The ABTS oxidation was followed spectroscopically using a Q798U/QUIMIS® UV/vis spectrometer. The general activity assay is described as follows: 1440 µL of 100 mM acetate buffer (pH 5), 20 µL of an aqueous ABTS solution (11 mg/mL), and 40 µL of laccase solutions ($1.25x10^{-3}$ mg/mL) were added sequentially into a glass cuvette (l = 0.5 cm). The absorbance was recorded for 3 minutes at 436 nm (ε_{436} = 29.200 $M^{-1}cm^{-1}$) at room temperature. This protocol was slightly varied to determine complex laccase/nanozeolite activities. Assays were carried out in 20 mL uncapped glass vials containing 2 mg of complex laccase/nanozeolite suspended in 1480 µL of 100 mM acetate buffer (pH 5) + 20 µL of an aqueous ABTS

solution (11 mg/mL). The suspension was magnetically stirred for 9.5 min, rapidly transferred to a centrifuge tube, centrifuged for 30 s (11,000 x g), the supernatant transferred to cuvette, and absorbance collected immediately, 10 min total reaction time. One unit (*u*) of the enzyme was defined as 1 μmol ABTS oxidized per minute under the stated assay condition. The enzymatic activity was denominated **U** (*u*/mL) or **Ů** (*u*/mg) for free or immobilized enzyme, calculated using the equations below [20]:

$$\mathbf{U} = Abs * V_t \ / \varepsilon * L * V_e * T * 10^3 * D$$

$$\mathbf{\mathring{U}} = Abs * V_t \ / \varepsilon * L * w_t * T * 10^3 * D$$

where **Abs**, is the absorbance at 436 nm; $\mathbf{V_t}$, is the total reaction volume (1.5 mL); $\mathbf{V_e}$, is the laccase solution volume; $\mathbf{w_t}$, is the added complex weight (mg); **ε**, is the molar extinction coefficient (29200 $M^{-1}cm^{-1}$); **L,** is the light path (0.5 cm); **T**, is the incubation time; $\mathbf{10^3}$, is the units correction factor; **D**, is the sample dilution, if necessary.

Optimum temperature, optimum pH, thermostability and pH stability were determined for free LPO, LAB and LAsp adjusting the described protocol. Stock solutions of transition metals (20, 40, 60, 80 and 100 mM) were prepared in 100 mM acetate buffer (pH 5) and used to verify their influence on the laccases activity at room temperature following the general protocol (stock solutions instead of just buffer). All assays run in triplicate if not otherwise stated.

2.7. Glycerol oxidation

The glycerol oxidation was performed following the method described by Liebminger *et al.* (2009)[12], with the pertinent modifications to our system. In a typical assay, 5 mL of solution prepared in 50 mM sodium acetate buffer, pH 5, containing glycerol (200 mM), TEMPO (30 mM), and amounts of in solution laccases (0.15 **U**) or immobilized

solid materials (catalyst weight with activity equivalent to 0.15 **U**). The reactions were carried out for 48 hours at room temperature (25 °C). Glycerol oxidation products were quantified using High Performance Liquid Chromatography, using an Agilent Technologies (Waldbronn, Germany), model 1220 Infinity with a Photodiode Array Detector, DAD. An Aminex HPX–87H (BioRad) 300 x 7.8 mm column was used. The mobile phase was a 4 mM H_2SO_4 solution in ultrapure water (18 Ω). Flow was adjusted to 0.5 $mLmin^{-1}$, and 20 µL of sample injected. Column incubated at 60 °C throughout 20 minutes chromatographic analysis.

3. Results and Discussion

3.1. Zeolitic supports characterization

The synthesis of the FAU/Na^+, FAU/Cu^{2+}, TS-1, ZSM-5, LTA and BEA nanozeolites were confirmed by comparing XRD patterns (Figure S1) and SEM images (Figure S2) with literature [24-29, 32, 33] as thoroughly described in previous studies [20, 21]. Particular attention was given to the FAU/Cu^{2+} material due to new observations regarding its content. FAU/Na^+ and FAU/Cu^{2+} SEM images and XRD patterns are contrasted in **Fig. 1**. Despite apparent similar morphologies revealed by SEM (**Fig. 1B** and **1C**), the XRD patterns presents significant differences (**Fig. 1A**). Previous this behavior has been assigned to a possible structure directing role of the copper ion on the Faujasite topology, which apparently shifted to a Gismondine (GIS) topology under ion exchange conditions [20]. However, in this study, an investigation has been carried out aiming to prove if the topology has indeed shifted or the XRD patterns are results of something else. Initially, the search on a XRD database was performed using the program **Match!*** [34]. Surprisingly, a mineral presented around

90% Bragg reflections matches with the FAU/Cu^{2+} ones. This mineral is a hydrous copper sulfate with the formula $Cu_3(SO_4)(OH)_4$ called antlerite, with characteristics infrared bands at 3570, 3490, 1153 and 1109 cm^{-1} [35]. These infrared bands can be found in the FAU/Cu^{2+} FTIR spectra while it is not present in the FAU/Na^{+} spectra (**Fig. 1D**). On the other hand, a group of bands in the 1000 – 400 cm^{-1} region, where characteristic zeolitic bands are found [36], can be observed for both materials. Moreover, Bragg reflections in 2θ equal 6° and 10°, characteristic of the faujasite material [20], are found in the copper exchanged material, but not in the antlerite pattern. This suggest that the FAU/Cu^{2+} material is actually composed of more than one topology, the faujasite topology and a copper sulfate topology. To verify on that TEM has been employed. **Fig. 2 A1** and **A2** shows dark field and bright field TEM data of the FAU/Cu^{2+} material, respectively. It is clear the presence of different shapes objects, where a globular-like morphology is in contrast with a rod-like morphology.

A small section from **Fig. 2A1**, where two particles of different shapes could be found (**Fig. 2B1**) was submitted to EDX analysis, in which oxygen (**Fig. 2B2**), silicon (**Fig. 2B3**), aluminum (**Fig. 2B4**), copper (**Fig. 2B5**) and sulphur (**Fig. 2B6**) were mapped out. It is evident that the globular-like particle is rich in silicon and aluminum, while the rod-like particle presents very low content of these elements. Meanwhile, oxygen, copper and sulphur are present in both particles, with oxygen found more intensively in the globular-shaped object and copper and sulphur in the rod-shaped object. The high aluminum and silicon content of the globular material allows inference that this is a zeolitic material, and the presence of copper spread uniformly though its structure indicates that the sodium from the FAU/Na^{+} zeolite has been replaced for copper cations, as expected in an ion exchange treatment. In contrast, the absence of

these elements in the other particles confirms a presence of a second phase in the FAU/Cu^{2+}. The presence of sulphur in both phases can be result of small layers of the copper sulfate mineral deposited onto the zeolitic phase. The second phase formation in an ion exchange process has been previously reported [37, 38]. Both studies attributed the mineral formation to harsh ion-exchange conditions (high temperature and copper concentration). Similar conditions were employed in this study (7 days, 80°C, 0.5 M $CuSO_4$), so the faujasite copper ion exchange has indeed led to a second phase formation rather than structure directing the FAU to GIS topology, and data strongly suggests antlerite as the secondary phase.

Fig. 1D also presents the FTIR spectra for the FAU/Na^+ and FAU/Cu^{2+} alkoxysilane functionalized (FAU/Na^+/APTMS and FAU/Cu^{2+}/APTMS) and cross-linked (FAU/Na^+/APTMS/GA and FAU/Cu^{2+}/APTMS/GA). New absorption bands are revealed when comparing spectra from each treatment stage. This can be associated with the modification groups used and can be assigned in all modified nanozeolites (Figure S3), providing evidence of effective treatments, as previously detailed [21].

3.2. Laccases characterization

The commercial laccases LPO, LAB and LAsp were spectroscopically characterized by means of their activity towards ABTS oxidation; varying parameters such as temperature, pH and chemical environment. **Fig. 3A** left shows the laccases' activity response when temperature was varied. Optimum temperatures around 60, 75 and 65 °C were found for LPO, LAB and LAsp, respectively. Other than temperature, pH is a relevant parameter to consider when working with laccases, commonly reported to be pH dependent with greater activity in acidic mediums [39]. **Fig. 3A** right illustrates the laccases pH dependence, and their optimum pH has been determined to be

around 3. Both optimum temperature and pH determined are in good agreement with literature [39-42].

Further, the thermostability and pH stability of the laccases were verified. The enzymes activities were checked over time for incubation temperatures of 30, 45 and 60 °C, at pH 4.5, **Fig. 3B**. In general, high instability is noted for LPO and LAsp, only stable at 30°C. On the other hand, LAB presented quite good stability even for higher temperatures. **Fig. 3C** presents the behavior of the laccases over time when incubated in pH 2, 3, 4, 5 and 6 buffer at 30 °C. LAsp is only stable at pH 6, in all other cases, fast activity reduction was observed. LPO is quite stable for pH values 4, 5 and 6, but moderate activity reduction was observed for pH 3. LAB, which had good temperature stability, is also stable for different pH values. Significant instability is noted for all laccases at pH 2.

The final stage of the free laccases characterization investigated whether some transition metal would interfere with the enzyme's activity. The enzymes activities were measured in the presence of varied concentrations (20 – 100 mM) of bivalent metals (Cu^{2+}, Zn^{2+}, Ni^{2+}, Co^{2+}, Mn^{2+} and Mg^{2+}). In general, the tested metals did not interfered or lead to moderate increase of enzyme activity, except for cobalt and copper, **Fig. 4**. The enzyme's responded negatively to cobalt. The higher the concentration of cobalt, the lower the enzyme relative activity. Interestingly, the presence of copper led to the most increase of all the enzyme's activities as the concentration was increased. It is known that copper enhances laccases activities [43, 44], due to the favorable equilibrium maintenance of the four copper atoms at the catalytic site, required for optimum performance.

3.3. Laccases immobilization and complexes characterization

The differently prepared nanozeolitic supports were tested for the laccase's immobilization. **Table 1** presents the immobilization results with regard to enzyme loading percentage, remaining activity (remaining activity in supernatant solution after immobilization process) and complexes activities. For comparative use, it is indicated the theoretical value that would be expected for the activity of the complexes if the entire enzyme content available was immobilized in the support and maintained 100 % of its activity (15000 μŮ), which is considerably higher than the activities of all complexes tested, even those that immobilized approximately the entire enzyme content available. This is mainly as a result of changing the catalytic system from homogeneous to heterogeneous. The dispersibility of an enzyme in solution is much superior to the dispersibility of nanozeolite complexes/enzymes. This is due to mass transfer limitations, which can critically affect the kinetics of a catalytic system [45]. Therefore, the activities of the complexes will be compared to each other, not with a supposed free enzyme equivalent.

All complexes showed some activity towards ABTS oxidation, however, the complexes with the copper containing support, FAU/Cu^{2+}/APTMS/GA, showed quite superior activity per milligram of complex, 1879 ± 45 μŮ – FAU/Cu^{2+}/APTMS/GA/LPO, 1535 ± 39 μŮ – FAU/Cu^{2+}/APTMS/GA/LAB, and 3166 ± 57 μŮ – FAU/Cu^{2+}/APTMS/GA/LAsp. The only other complex that presented comparatively good activity was the complex BEA/APTMS/GA/LAsp (2133 ± 55 μŮ). All other complexes gave activities lower than 400 μŮ. Notwithstanding, the FAU/Cu^{2+}/APTMS/GA/laccases complexes were chosen for further complex characterization with regard to optimum reactional conditions and stability.

The selected complexes were submitted for the ABTS oxidation varying temperatures (30, 45 and 60 °C) and pH (3, 4 and 5), and the relative activities are illustrated in **Fig. 5A**. All complexes presented optimum catalytic performance at 30 °C and pH 3. However, for this pH, the complexes activities were reduced at higher temperatures, more drastically for the LAsp complex, showing no activity at 60 °C. LPO and LAB complexes presented around 30% and 60% the activities at pH 3/30 °C, respectively. In general, each complex showed a unique response to the same experimental conditions. While the optimum was also at pH 3 for LAB at 45 °C, for LPO and LAsp, the optimum was observed at pH 4. In addition, at 60 °C, the LPO complex showed very similar activities for the tested pH, whilst LAB and LAsp showed optimum at pH 4. It was clear that the immobilized and free enzymes behaved very differently. To analyze whether immobilization led to more stable enzymes, the thermostability of the complexes were assayed at pH 3 and 30 or 45 °C, **Fig. 5B**. The single most striking observation to emerge from the data analysis was that the complexes were not stable at pH 3 for long periods, independently of temperature. The data presented so far was used to define which would be the appropriate conditions for the selected complexes application to the proposed glycerol TEMPO/mediated oxidation. Based on optimum performances and stability, pH 5 and 25 °C were initially used for this reaction.

3.4. Glycerol oxidation

Table 2 presents the glycerol oxidation results. Initially, the free laccases were tested for the proposed TEMPO-mediated oxidation of glycerol. LPO presented the highest conversion yield (81.54%) in 48 hours, followed by LAsp (28.77%) and LAB (3.19%) at 25 °C. Despite highest conversion, LPO selectivity to glyceraldehyde

(57.10%) was lower than LAsp (78.00%), with secondary most abundant product being glyceric acid (21.00% conversion / 25.75% selectivity) and glyoxylic acid (3.30 conversion / 11.47 selectivity), respectively. In contrast, LAB yield was only 3.19%, with high selectivity to glyceraldehyde (97.81%). In terms of production, all tested complexes yielded less than 5% conversion, and similarly to LAB, presented high selectivity to glyceraldehyde (>88%).

The oxidation products for free LPO was followed up over time to get insights concerning the glycerol oxidation pathway, **Fig. 6**. In the first 3 hours, the reaction mainly produced glyceraldehyde (GcAd), and very small amounts of glyoxylic (GoAc), glyceric (GAc) and oxalic (OAc) acids. In the next 3 hours, the amount of GcAd approximately doubled, while GoAc and GAc yields increased about 4 and 5-folds, respectively. Noteworthy, from this set of data was the production of three compounds, GcAd, GAc and GoAc. The yield of GcAd increased in the first 24 hours, but reduced in the next 24 hours. GAc amount was increased during the complete interval follow up. GoAc amount increased in the first 6 hours, then reduced in the next 6 hours, then increased again for the rest of the reaction. Based on these results, we can suggest that LPO TEMPO-mediated reaction followed a similar pathway to the reported by Zhou et al. (2008)[1], which considered that glycerol would first be oxidized to glyceraldehyde, which would then in sequence be converted to glyceric acid, and glyceric acid to tartronic acid. Tartronic acid on its turn could be transformed into mesoxalic acid, or oxalic acid, or glyoxylic acid. Overall, a series of different reactions was in place in this study, leading to non-selective glycerol oxidation, which is in agreement with the study reported by Liebminger et al. (2009)[12].

Table 3 summarizes the main results of the studies that previously addressed this system compared with the results in this study. Different laccases, supports, immobilization methods and reaction conditions were tested. It is clear that only free enzymes have led to high yields of oxidation products. However, the amount of free enzyme (based on activity) used in this study is lower than the amount used for the other studies, in the order of 6 folds. This allows us to point out that both, LPO and LAsp, which have never before been studied in this context, are potential catalysts for the proposed reaction. On the other hand, when attention is given to studies in which the laccases were immobilized, none presented high conversions – less than 30% – and in agreement with our study. Certainly, greater or lesser residual activity of immobilized enzymes is directly related to the physical-chemical interactions between enzymes and supports, as well as the interaction with the mediators involved. To shed light on these results, CW EPR spectroscopy was applied.

3.5. EPR analysis

Laccase has an EPR spectrum indicating the presence of a combination of T1 and T2 catalytic copper centers [46]. **Fig. 7A-F** shows X-band EPR spectra obtained for the laccase/nanozeolite complexes (solid lines) compared with the spectra of the enzyme-free nanozeolites (dotted lines). Simulations were performed to determine the spin Hamiltonian parameters and are presented in **Table 4** (Figure S4). In all cases, significant differences are evident in the spectra when comparing the *g* and hyperfine values of the T1 and T2 coppers catalytic sites, with the FAU/Cu^{2+}/APTMS/GA/LAsp and LTA/APTMS/GA/LAsp, in which the high concentration of Cu^{2+} present in the zeolite suppressed the signals of the laccase coppers.

To help us understand the results, comparison was made to the EPR spectra of the laccase samples in frozen solution at pH 7 and 4.5, and untreated at pH 7 (**Fig. 7G**). The frozen solution laccase EPR spectra , again, show the typical spectral features of blue laccases [46, 47] with both T1 and T2 copper sites being present. The treated enzyme at pH 7 presents a shift in the isolated resonances characteristic of copper T2 to smaller $g_{//}$ and $A_{//}$ values (arrow indicate the shift); the parallel hyperfine coupling constant is 220.2 x 10^{-4} cm^{-1} for the treated enzyme at pH 4.5 while the constant determined for the enzyme at pH 7 is 170.1 x 10^{-4} cm^{-1}. This indicates variation of the unpaired electron delocalization on Cu^{2+} as a function of pH. The untreated sample, pH 7, presented a spectrum with resonances close to those observed for the treated enzyme at pH 7 with subtle changes in line width.

Interestingly, the *g* and *A* values of the T2 copper site of the immobilized samples most closely resemble the values of the treated/untreated laccase at pH 7(**Fig. 7H)**. This is most evident for the $A_{//}$ value of BEA/APTMS/GA/LAsp complex with its almost identical value to the untreated enzyme. It is possible that this arises from the distortion of the coordination geometry of the T2 copper site (Figure S5). The parameters for the T1 copper site show less variation.

The data in **Fig. 7** indicate a strong influence of pH on the EPR spectroscopy of the LAsp laccase, and in addition, that the spectral resonances observed for the immobilized enzyme are very close to those observed for the enzyme at pH 7. This raises the hypothesis that the microenvironments of immobilized enzymes are highly sensitive to changes in pH. Moreover, this could explain the reduction of the catalytic activity of the laccases immobilized in zeolites, since the data clearly indicate optimal activity for the free enzymes at acidic pH. And, although the reaction medium for glycerol oxidation

was adjusted to pH 4.5, it does not necessarily reflect the pH of the enzymatic microenvironments close to the zeolite surface. Overall, the EPR study, reveals significant changes to the laccase copper catalytic sites on immobilization.

4. Conclusions

The different synthetized nanozeolites could successfully immobilize the tested laccases. Faujasite nanozeolite ion exchanged with Cu^{2+} and functionalized with APTMS and cross-linked with GA successfully immobilized the laccases LPO, LAsp and LAB resulting in different nanozeolite-lacases complexes with great activity towards ABTS. Oxidation of glycerol to glyceraldehyde, glyceric acid, among other products, was achieved. Although the application of the selected laccase/nanozeolite catalysts to glycerol TEMPO-mediated oxidation did not result in high yields of conversion, significant selectivity to glyceraldehyde was observed (up to 100%). In contrast, free enzymes led to higher yields of conversion, but a plethora of different products were obtained. This suggests that the immobilization of laccases into nanozeolites generates a promising catalyst for the controlled TEMPO-mediated glycerol oxidation. EPR spectroscopy data revealed a significant change of the spin Hamiltonian parameters in the parallel region of the T2 copper site depending on pH. In the free form, LAsp $g_{//}$ and $A_{//}$ were 2.270 and 220.2 x 10^{-4} cm^{-1}, respectively, at pH 4.5, whilst at pH 7 these values varied to 2.275 and 170.1 x 10^{-4} cm^{-1}. The spectral features of the immobilized LAsp has approximately the same values for the free enzyme at pH 7, and the BEA/APTMS/GA/LAsp complex (g 2.275 and 173.4 x 10^{-4} cm^{-1}). These results in principle could explain the low effectiveness of the complexes observed not only in this study but also in other similar systems reported in the literature. Therefore, the study suggests that in the future for the designing of effective catalysts of this

immobilized laccase/TEMPO-mediated glycerol oxidation system, attention should be paid to the microenvironment of this system.

Acknowledgements

The authors are thankful to the financial support from the São Paulo Research Foundation (FAPESP) (Grant numbers: 2016/24303-0 and 2018/21483-3) and a Leverhulme Fellowship (RF-2019-474\4) to Fielding.

Appendix A. Supplementary data

Supporting information contains extra XRD, SEM and FTIR characterization data of the nanozeolitic supports, EPR simulations plots against experimental spectra, and structural analysis of the MtL(LAsp) catalytic center.

References

[1] C.-H.C. Zhou, J.N. Beltramini, Y.-X. Fan, G.Q.M. Lu, Chemoselective catalytic conversion of glycerol as a biorenewable source to valuable commodity chemicals, Chemical Society Reviews, 37 (2008) 527-549.

[2] G. Dodekatos, S. Schünemann, H. Tüysüz, Recent advances in thermo-, photo-, and electrocatalytic glycerol oxidation, ACS Catalysis, 8 (2018) 6301-6333.

[3] A. Behr, J. Eilting, K. Irawadi, J. Leschinski, F. Lindner, Improved utilisation of renewable resources: new important derivatives of glycerol, Green Chemistry, 10 (2008) 13-30.

[4] J.A. Bernatchez, R. Paul, E.P. Tchesnokov, M. Ngure, G.L. Beilhartz, A.M. Berghuis, R. Lavoie, L. Li, A. Auger, R.A. Melnyk, Derivatives of mesoxalic acid block

translocation of HIV-1 reverse transcriptase, Journal of Biological Chemistry, 290 (2015) 1474-1484.

[5] R. Ciriminna, M. Pagliaro, Oxidation of tartronic acid and dihydroxyacetone to sodium mesoxalate mediated by TEMPO, Tetrahedron letters, 45 (2004) 6381-6383.

[6] D.T. Johnson, K.A. Taconi, The glycerin glut: Options for the value-added conversion of crude glycerol resulting from biodiesel production, Environmental Progress, 26 (2007) 338-348.

[7] J.N. Chheda, G.W. Huber, J.A. Dumesic, Liquid-phase catalytic processing of biomass-derived oxygenated hydrocarbons to fuels and chemicals, Angewandte Chemie International Edition, 46 (2007) 7164-7183.

[8] J.C. Beltrán-Prieto, K. Kolomazník, J. Pecha, A Review of Catalytic Systems for Glycerol Oxidation: Alternatives for Waste Valorization, Australian Journal of Chemistry, 66 (2013) 511-521.

[9] C.S. Hong, S.Y. Chin, C.K. Cheng, M.M. Sabri, G.K. Chua, Enzymatic Conversion of Glycerol to Glyceric Acid with Immobilised Laccase in Na-Alginate Matrix, Procedia Chemistry, 16 (2015) 632-639.

[10] A. Villa, N. Dimitratos, C.E. Chan-Thaw, C. Hammond, L. Prati, G.J. Hutchings, Glycerol Oxidation Using Gold-Containing Catalysts, Accounts of Chemical Research, 48 (2015) 1403-1412.

[11] R. Ciriminna, M. Pagliaro, One-Pot Homogeneous and Heterogeneous Oxidation of Glycerol to Ketomalonic Acid Mediated by TEMPO, Advanced Synthesis & Catalysis, 345 (2003) 383-388.

[12] S. Liebminger, M. Siebenhofer, G. Guebitz, Oxidation of glycerol by 2, 2, 6, 6-tetramethylpiperidine-N-oxyl (TEMPO) in the presence of laccase, Bioresource technology, 100 (2009) 4541-4545.

[13] C.S. Hong, C.C.Y. Lau, C.Y. Leong, G.K. Chua, S.Y. Chin, A comparison of entrapped and covalently bonded laccase: Study of its leakage, reusability, and the catalytic efficiency in TEMPO-mediated glycerol oxidation, Biocatalysis and Biotransformation, 36 (2018) 352-361. [14] C.S. Hong, S.Y. Chin, C. Kui Cheng, G.K. Chua, Selective oxidation of glycerol to mesoxalic acid by laccase/2, 2, 6, 6-tetramethylpiperidine-N-oxyl system: Effect of process conditions and the kinetic modeling, Chemical Engineering Communications, 206 (2019) 1645-1660.

[15] A. M. Barreca, M. Fabbrini, C. Galli, P. Gentili, S. Ljunggren, Laccase/mediated oxidation of a lignin model for improved delignification procedures, Journal of Molecular Catalysis B: Enzymatic**,** 26 (2003) 105-110.

[16] A. Potthast, T. Rosenau, C. L. Chen, J. S. Gratzl, A novel method for conversion of benzyl alcohols to benzaldehydes by laccase-catalysed oxidation, Journal of Molecular Catalysis A: Chemical, 108 (1996) 5-9.

[17] M. Fabbrini, C. Galli, P. Gentili, D. Macchitella, An oxidation of alcohols by oxygen with the enzyme laccase and mediation by TEMPO, Tetrahedron Letters, 42 (2001) 7551-7553.

[18] I. Matijošytė, I. W. C. E. Arends, S. de Vries, R. A. Sheldon, Preparation and use of cross-linked enzyme aggregates (CLEAs) of laccases. Journal of Molecular Catalysis B: Enzymatic**,** 62 (2010) 142-148.

[19] N.A. Daronch, M. Kelbert, C.S. Pereira, P.H.H. de Araújo, D. de Oliveira, Elucidating the choice for a precise matrix for laccase immobilization: a review, Chemical Engineering Journal, (2020) 125506.

[20] A. de Vasconcellos, J.B. Laurenti, A.H. Miller, D.A. da Silva, F.R. de Moraes, D.A.G. Aranda, J.G. Nery, Potential new biocatalysts for biofuel production: the fungal lipases of *Thermomyces lanuginosus* and *Rhizomucor miehei* immobilized on zeolitic

supports ion exchanged with transition metals, Microporous and Mesoporous Materials, 214 (2015) 166-180.

[21] A. de Vasconcellos, A.H. Miller, D.A.G. Aranda, J.G. Nery, Biocatalysts based on nanozeolite-enzyme complexes: Effects of alkoxysilane surface functionalization and biofuel production using microalgae lipids feedstock, Colloids and Surfaces B: Biointerfaces, 165 (2018) 150-157.

[22] L. Tosheva, V.P. Valtchev, Nanozeolites: Synthesis, crystallization mechanism, and applications, Chemistry of Materials, 17 (2005) 2494-2513.

[23] B.Z. Zhan, M.A. White, M. Lumsden, J. Mueller-Neuhaus, K.N. Robertson, T.S. Cameron, M. Gharghouri, Control of particle size and surface properties of crystals of NaX zeolite, Chemistry of Materials, 14 (2002) 3636-3642.

[24] B.Z. Zhan, M.A. White, K.N. Robertson, T.S. Cameron, M. Gharghouri, A novel, organic-additive-free synthesis of nanometer-sized NaX crystals, Chemical Communications, (2001) 1176-1177.

[25] C.S. Cundy, J.O. Forrest, Some observations on the preparation and properties of colloidal silicalites Part II: Preparation, characterisation and properties of colloidal silicalite-1, TS-1, silicalite-2 and TS-2, Microporous and Mesoporous Materials, 72 (2004) 67-80.

[26] C.S. Cundy, J.O. Forrest, R.J. Plaisted, Some observations on the preparation and properties of colloidal silicalites. Part 1: synthesis of colloidal silicalite-1 and titanosilicalite-1 (TS-1), Microporous and Mesoporous Materials, 66 (2003) 143-156.

[27] E. Biemmi, T. Bein, Assembly of Nanozeolite Monolayers on the Gold Substrates of Piezoelectric Sensors, Langmuir, 24 (2008) 11196-11202.

[28] M. Jafari, A. Nouri, M. Kazemimoghadam, T. Mohammadi, Investigations on hydrothermal synthesis parameters in preparation of nanoparticles of LTA zeolite with the aid of TMAOH, Powder technology, 237 (2013) 442-449.

[29] O. Larlus, S. Mintova, S.T. Wilson, R.R. Willis, H. Abrevaya, T. Bein, A powerful structure-directing agent for the synthesis of nanosized Al- and high-silica zeolite Beta in alkaline medium, Microporous and Mesoporous Materials, 142 (2011) 17-25.

[30] S. Stoll, A. Schweiger, EasySpin, a comprehensive software package for spectral simulation and analysis in EPR, Journal of magnetic resonance, 178 (2006) 42-55.

[31] M.M. Bradford, Rapid and sensitive method for quantitation of microgram quantities of protein utilizing principle of protein-dye binding, Analytical Biochemistry, 72 (1976) 248-254.

[32] R. Van Grieken, J.L. Sotelo, J.M. Menendez, J.A. Melero, Anomalous crystallization mechanism in the synthesis of nanocrystalline ZSM-5, Microporous and Mesoporous Materials, 39 (2000) 135-147.

[33] G. Majano, S. Mintova, O. Ovsitser, B. Mihailova, T. Bein, Zeolite Beta nanosized assemblies, Microporous and Mesoporous Materials, 80 (2005) 227-235.

[34] Crystal Impact, Match! Phase Identification from Powder Diffraction, https://www.crystalimpact.com/match/, 2021 (accessed 25 August 2021).

[35] A.H. Zittlau, Q. Shi, J. Boerio-Goates, B.F. Woodfield, J. Majzlan, Thermodynamics of the basic copper sulfates antlerite, posnjakite, and brochantite, Chemie der Erde-Geochemistry, 73 (2013) 39-50.

[36] E.M. Flanigen, H. Khatami, H.A. Szymanski, Infrared structural studies of zeolite frameworks, Molecular Sieve Zeolites, 16 (1971) 201-229. [37] Y. Bhawe. I: Materials for thermochemical water splitting. II: Structure-property relations for the zeolite

catalyzed conversion of methanol to light olefins, Doctoral dissertation, California Institute of Technology, 2013.

[38] N.Q. Long, H.T. Vuong, H.K.P. Ha, W. Kuniawan, H. Hinode, T. Baba, Preparation, characterization and H2S adsorptive removal of ion-exchanged zeolite X, ASEAN Engeneering Journal,, 5 (2016) 4-14.[39] F. Tonin, R. Melis, A. Cordes, A. Sanchez-Amat, L. Pollegioni, E. Rosini, Comparison of different microbial laccases as tools for industrial uses, New biotechnology, 33 (2016) 387-398.

[40] L. Liu, Z. Lin, T. Zheng, L. Lin, C. Zheng, Z. Lin, S. Wang, Z. Wang, Fermentation optimization and characterization of the laccase from Pleurotus ostreatus strain 10969, Enzyme and Microbial Technology, 44 (2009) 426-433.

[41] L. Zhilin, S. Weilong, L. Wei, L. Hesheng, Immobilization of *Agaricus Bisporus* Laccase on Ceramic-Chitosan Composite Support and Their Properties: Potential for Oily Wastewater Treatment, China Petroleum Processing & Petrochemical Technology, 18 (2016) 51-60.

[42] L. Lloret, F. Hollmann, G. Eibes, G. Feijoo, M.T. Moreira, J.M. Lema, Immobilisation of laccase on Eupergit supports and its application for the removal of endocrine disrupting chemicals in a packed-bed reactor, Biodegradation, 23 (2012) 373-386.

[43] A. Mukhopadhyay, A.K. Dasgupta, K. Chakrabarti, Thermostability, pH stability and dye degrading activity of a bacterial laccase are enhanced in the presence of Cu 2 O nanoparticles, Bioresource technology, 127 (2013) 25-36.

[44] J. Si, F. Peng, B. Cui, Purification, biochemical characterization and dye decolorization capacity of an alkali-resistant and metal-tolerant laccase from *Trametes pubescens*, Bioresource technology, 128 (2013) 49-57.

[45] H.R. Wehaidy, M.A. Abdel-Naby, H.M. El-Hennawi, H.F. Youssef, Nanoporous Zeolite-X as a new carrier for laccase immobilization and its application in dyes decolorization, Biocatalysis and agricultural biotechnology, 19 (2019) 101135.

[46] S.M. Jones, E.I. Solomon, Electron transfer and reaction mechanism of laccases, Cellular and molecular life sciences, 72 (2015) 869-883.

[47] A. Gupta, I. Nederlof, S. Sottini, A.W.J.W. Tepper, E.J.J. Groenen, E.A.J. Thomassen, G.W. Canters, Involvement of Tyr108 in the enzyme mechanism of the small laccase from *Streptomyces coelicolor*, Journal of the American Chemical Society, 134 (2012) 18213-18216.

Figure Captions

Fig. 1. Characterization of the supports. XDR patterns (**A**) and SEM images of FAU/Na^+ (**B**) and FAU/Cu^{2+} (**C**) supports. FTIR spectra of these two materials compared with its APTMS alkoxysilane functionalized and GA cross-linked derivatives spectra (**D**).

Fig. 2. TEM data for the sample FAU/Cu^{2+}, dark field (A1) and bright field (A2). Energy dispersive X-ray (EDX) mapping analysis of the FAU/Cu^{2+} material (B1): oxygen (B2), silicon (B3), aluminum (B4), copper (B5), and sulphur (B6).

Fig. 3. Biochemical characterization of the LPO, LAB and LAsp laccases. (A) Optimum temperatures (right) and pH (left) at 45°C. (B) Thermostability at the temperatures 30, 45 and 60 °C, pH 5. (C) pH stability at pH 2, 3, 4, 5 and 6 (30°C).

Fig. 4. Laccases activities in the presence of metal transition cations at 25 °C. Room temperature, pH 5.0 (100 mM acetate buffer).

Fig. 5. (A) Temperature and pH influence on FAU/Cu^{2+}/APTMS/GA/laccases complexes activities. **(B)** Thermostability of the FAU/Cu^{2+}/APTMS/GA/laccases complexes at 30 and 45 °C.

Fig. 6. Glycerol oxidation follow up using free LPO. Oxalic acid (OAc), mesoxalic acid (MAc), tartronic acid (TAc), glyoxylic acid (GoAc), glyceric acid (GAc) and glyceraldehyde (GcAd) quantities were determined by HPLC after 3, 6, 12, 24 and 48 hours reaction at room temperature.

Fig. 7. X-band EPR spectra of the nanozeolites with (solid lines) and without (dotted lines) immobilized LAsp (A to F). X-band EPR spectra of treated LAsp at pH 7 and 4.5 compared with the untreated enzyme at pH 7 (G). Positions of T1 and T2 hyperfine are marked. Comparison of the parallel region of the LAsp/nanozeolites complexes (solid lines 7A – F) with the spectra of the treated LAsp at pH 7 (7G, black line) and untreated (7G, blue line) (H). Highlighted regions and arrows indicate shifts.

Table 1. Amount of laccase immobilized on the zeolitic supports and their enzymatic activity after immobilization.

Support	**Laccase**	**Immobilization / %**	**Residual Activity / %**	**Complex Activity / μŮ**
HYPOTHETICAL SYSTEM [a]		100	0	15000
FAU/Na^{+}/APTMS/GA	LPO	94 ± 32[c]	0	86 ± 5
	LAB	55 ± 30[c]	0	204 ± 11
	LAsp	39 ± 2	86 ± 3	291 ± 13
TS-1/APTMS/GA	LPO	84 ± 25[c]	0	58 ± 4
	LAB	63 ± 21[c]	0	99 ± 4
	LAsp	88 ± 4	6.2 ± 0.5	364 ± 16
ZSM-5/APTMS/GA	LPO	88 ± 35[c]	0	276 ± 14
	LAB	78 ± 33[c]	0	8 ± 2

	LAsp	92 ± 4	0	25 ± 3
LTA/APTM/GA	LPO	NR[b]	NR	NR
	LAB	NR	NR	NR
	LAsp	26 ± 2	93.7 ± 0.3	258 ± 13
BEA/APTMS/GA	LPO	NR	NR	NR
	LAB	NR	NR	NR
	LAsp	94 ± 4	0.8 ± 0.2	2133 ± 55
FAU/Cu^{2+}/APTMS/GA	LPO	85 ± 25[c]	0	1879 ± 45
	LAB	90 ± 30[c]	0	1535 ± 39
	LAsp	90 ± 3	9.3 ± 0.4	3166 ± 57

[a] HYPOTHETICAL SYSTEM – if 100% of the enzyme was immobilized in the support and maintained 100 % of the activity it had in its free form, the complex formed would present activity of 15000 μŮ, regardless of the support or enzyme tested because the amount of enzyme available was adjusted based on its respective specific activities, and constant for all assays.

[b] NR - not realized

[c] Statistically it was not possible to obtain replicas that did not exceed the acceptable error – tests were repeated at least five times.

Table 2. Glycerol conversion (%) and product selectivity (%) in a free or immobilized laccase/TEMPO-mediated glycerol oxidation after 48 h.

Catalyst	**Product**	**Conversion / %**	**Selectivity / %**
		FREE ENZYMES	
LAsp [a,b]	Oxalic acid	1.57	5.46
	Mesoxalic acid	0.24	0.83
	Tartronic Acid	0.09	0.31
	Glyoxylic acid	3.30	11.47
	Glyceric acid	1.13	3.93
	Glyceraldehyde	22.44	78.00
	total	**28.77**	-
LPO [a,b]	Oxalic acid	1.95	2.39
	Mesoxalic acid	2.90	3.56
	Tartronic Acid	2.70	3.31
	Glyoxylic acid	6.43	7.89
	Glyceric acid	21.00	25.75
	Glyceraldehyde	46.56	57.10
	total	**81.54**	-

LAB [a,b]	Oxalic acid	0.07	2.19
	Glyceraldehyde	3.12	97.81
	total	**3.19**	100
	IMMOBILIZED ENZYMES		
A [c]/LAsp [b]	Oxalic acid	0.08	4.06
	Glyceraldehyde	1.89	95.94
	total	**1.97**	-
A [c]/LPO [b]	Oxalic acid	0.08	1.64
	Glyceraldehyde	4.79	98.36
	total	**4.87**	-
A [c]/LAB [b]	Oxalic acid	0.08	4.19
	Glyceraldehyde	1.83	95.81
	total	**1.91**	-
A [c]/LAsp [d]	Oxalic acid	0.17	11.64
	Glyceraldehyde	1.29	88.36
	total	**1.46**	-
A [c]/LPO [d]	Oxalic acid	0.20	8.44
	Glyceraldehyde	2.17	91.56
	total	**2.37**	-
A [c]/ /LAB [d]	Oxalic acid	0.11	8.94
	Glyceraldehyde	1.12	91.06
	total	**1.23**	-
B [c]/LAsp [b]	Glyceraldehyde	1.88	100
	total	**1.88**	-
	SUPPORT with no ENZYME		
A[e]	No products verified		
B[e]	No products verified		

[a] Free enzyme (amount of enzyme with activity equivalent to the activity of the respective enzyme complex with support A).
[b] 25 °C .
[c] Enzyme immobilized onto the supports: A - FAU/Cu^{2+}/APTMS/GA and B - BEAc/APTMS/GA.

[d] 45 °C. [e] Support only.

Table 3. Comparing the experimental conditions and production from the laccase/TEMPO-mediated glycerol oxidation reactions reported in the literature with the present work.

Laccase	Support	Experimental conditions					Conversion / % [b]	Selectivity / % [b]	Immobilization Method	Ref.
		pH	T / °C	t / h	[TEMPO]:[GLY]	Catalyst				
T. hirsuta	Free form	4.5	25	24	3:10	10 *U*/mL	70	23.4 – GcAd 23.4 – GAc 12.8 – TAc 19.1 – MAc	-	[12]
	Alumina *pellets*	4.5	25	24	3:10	0.1 *U*/mL	10	N.I.[a]	covalent binding	
T. versicolor	Sodium alginate	4.5	25	24	3:10	20 mg/mL[c]	30	23 – GAc 67 – GcAd	entrapment	[9]
	Free form	4.5	25	24	3:10	N.I.	40	75 – GcAd 20 – GAc	-	
	Sodium alginate	4.5	25	24	3:10	2 mg/mL[c]	27	85 – GcAd 9 – GAc	entrapment	[13]
	Alumina *pellets*	4.5	25	24	3:10	2 mg/mL[c]	8	>90 – GcAd	covalent binding	
	Free form	4.5	25	76	3:10	10 *U*/mL	76	30 – GAc 30 - MAc 26 – GcAd	-	[14]
	Free form	5.5	19	76	3:1	10 *U*/mL	~100	90 - MAc	-	
P. ostreatus	Free form	4.5	25	48	3:10	0.15 *U*/mL	82	57 – GcAs 26 – GAc	-	This work
	FAU/Cu^{2+}/APTMS/GA	4.5	25	48	3:10	0.15 *U*/mL	< 5	>98 GcAd	covalent binding	
Aspergillus sp	Free form	4.5	25	48	3:10	0.15 *U*/mL	29	78 – GcAd 11.5 – GoAc	-	
	FAU/Cu^{2+}/APTMS/GA	4.5	25	48	3:10	0.15 *U*/mL	< 2	>95 – GcAd	covalent binding	

[a] N.I. – not informed GAc - glyceric acid GoAc - glyoxylic acid GcAd- glyceraldehyde MAc - mesoxalic acid TAc - tartronic acid

[b] Conversion and selectivity values were approximated from the figures when not explicitly reported in the texts, and error bars not considered.

[c] It was not possible to determine from the procedures described the complexes' activities (*U*/mg), and thus determine the *U*/mL activity used to study the reactions.

Table 4. *g* Values and hyperfine coupling constant ***A*** for laccase T1 and T2 copper centers.

Sample	Copper T1				Copper T2[a]				T1:T2
	$g_{\|\|}$	$g_{\perp}$	$A_{\|\|}$	$A_{\perp}$	$g_{\|\|}$	$g_{\perp}$	$A_{\|\|}$	$A_{\perp}$	
Treated LAsp pH 7	2.211	2.060	86.7	16.7	2.275	2.046	170.1	16.7	1:0.7
Treated LAsp pH 4.5	2.200	2.064	91.7	16.7	2.270	2.065	220.2	16.7	1:0.7
Untreated LAsp pH 7	2.195	2.065	86.7	16.7	2.249	2.057	183.5	16.7	0.5:1
FAU/Na^+/APTMS/GA/LASP	2.197	2.064	91.7	16.7	2.245	2.048	186.7	16.7	0.6:1
BEA/APTMS/GA/LAsp[b]	2.219	2.065	86.7	16.7	2.275	2.055	173.4	16.7	0.7:1

[a] Hyperfine coupling constant ***A*** are expressed as wave numbers (cm^{-1}) with multiplication factor 10^{-4}. Parameters $A_{||}$ = 1.67 and $A_{\perp}$ = 13.3 were used for the superhyperfine interaction of copper T2 with ^{14}N of the coordinated histidines. [b] The EPR parameters for TS-1/APTMS/GA/LAsp and ZSM-5/GA/LAsp are within experimental error. FAU/Cu^{2+}/APTMS/GA/LAsp and LTA/APTMS/GA/LAsp spectra couldn't be simulated due to copper doping or metal impurities, respectively.

Figure 1

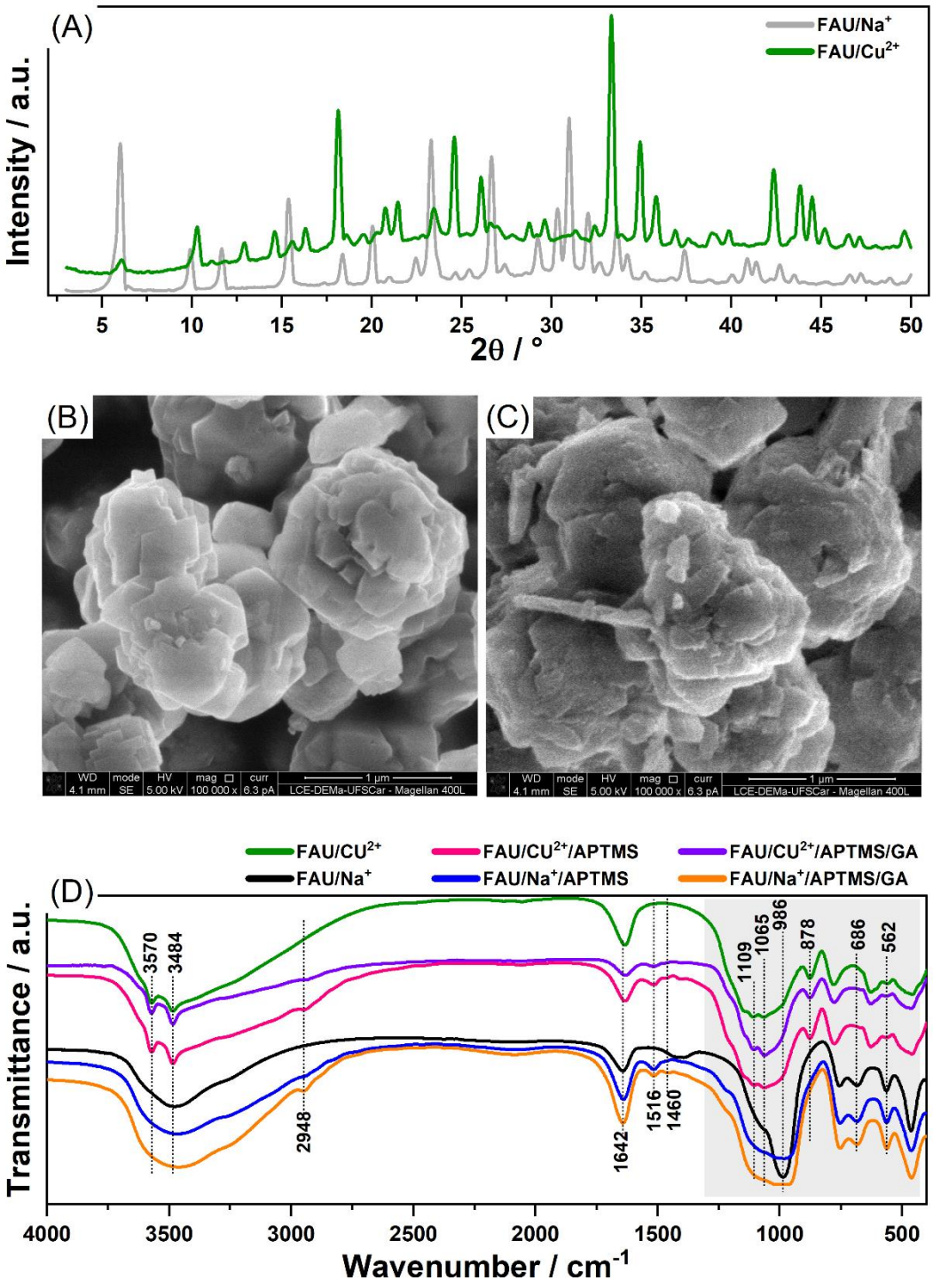
(A)
FAU/Na+
FAU/Cu2+
Intensity / a.u.
5
10
15
20
25
30
35
40
45
50
2θ / °
(B)
(C)
WD 4.1 mm
mode SE
HV 5.00 kV
mag 100 000 x
curr 6.3 pA
1 µm
LCE-DEMa-UFSCar - Magellan 400L
FAU/CU2+
FAU/CU2+/APTMS
FAU/CU2+/APTMS/GA
FAU/Na+
FAU/Na+/APTMS
FAU/Na+/APTMS/GA
(D)
Transmittance / a.u.
3570
3484
2948
1642
1516
1460
1109
1065
986
878
686
562
4000
3500
3000
2500
2000
1500
1000
500
Wavenumber / cm-1

Figure 2

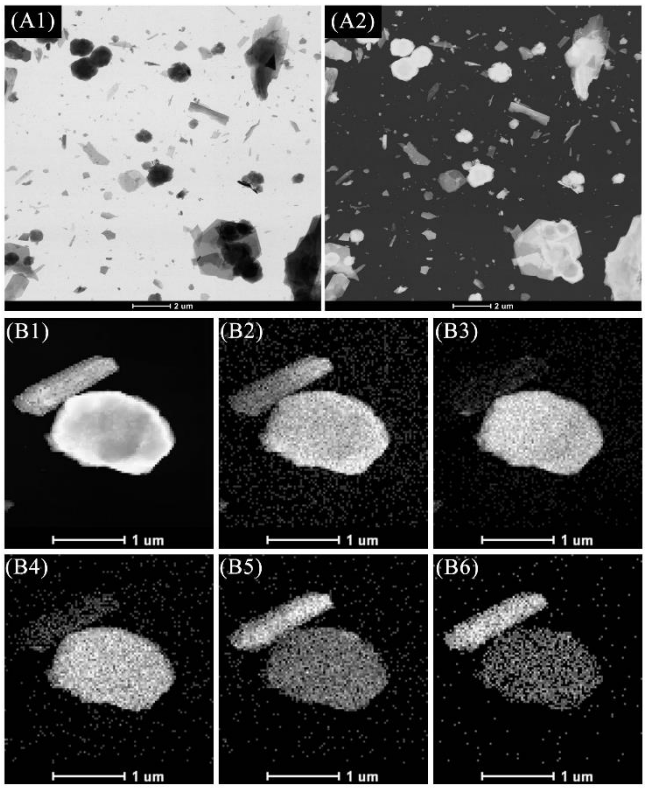

Figure 3

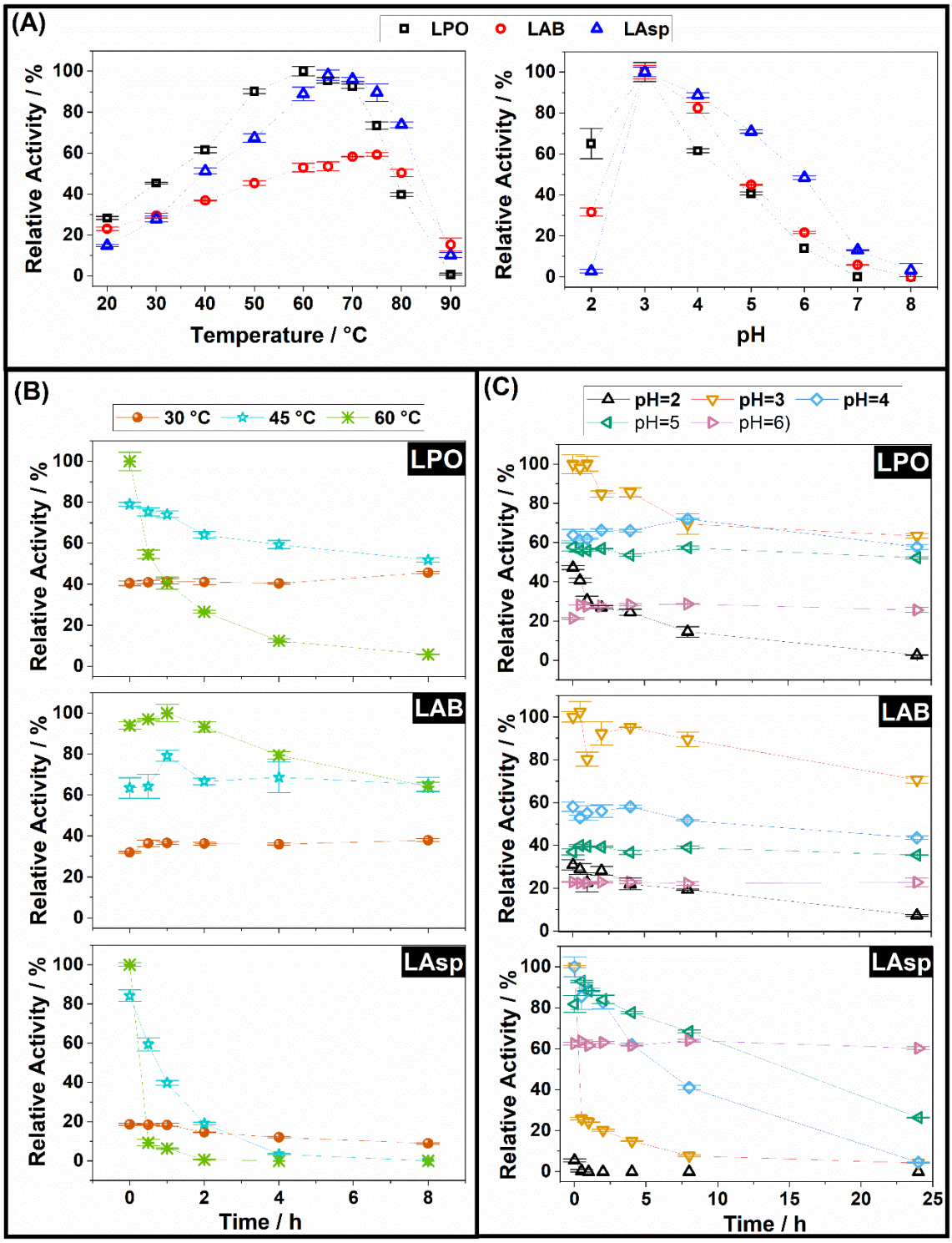
(A)
LPO
LAB
LAsp
Relative Activity / %
Temperature / °C
pH
(B)
30 °C
45 °C
60 °C
LPO
LAB
LAsp
Time / h
(C)
pH=2
pH=3
pH=4
pH=5
pH=6)
Time / h

Figure 4

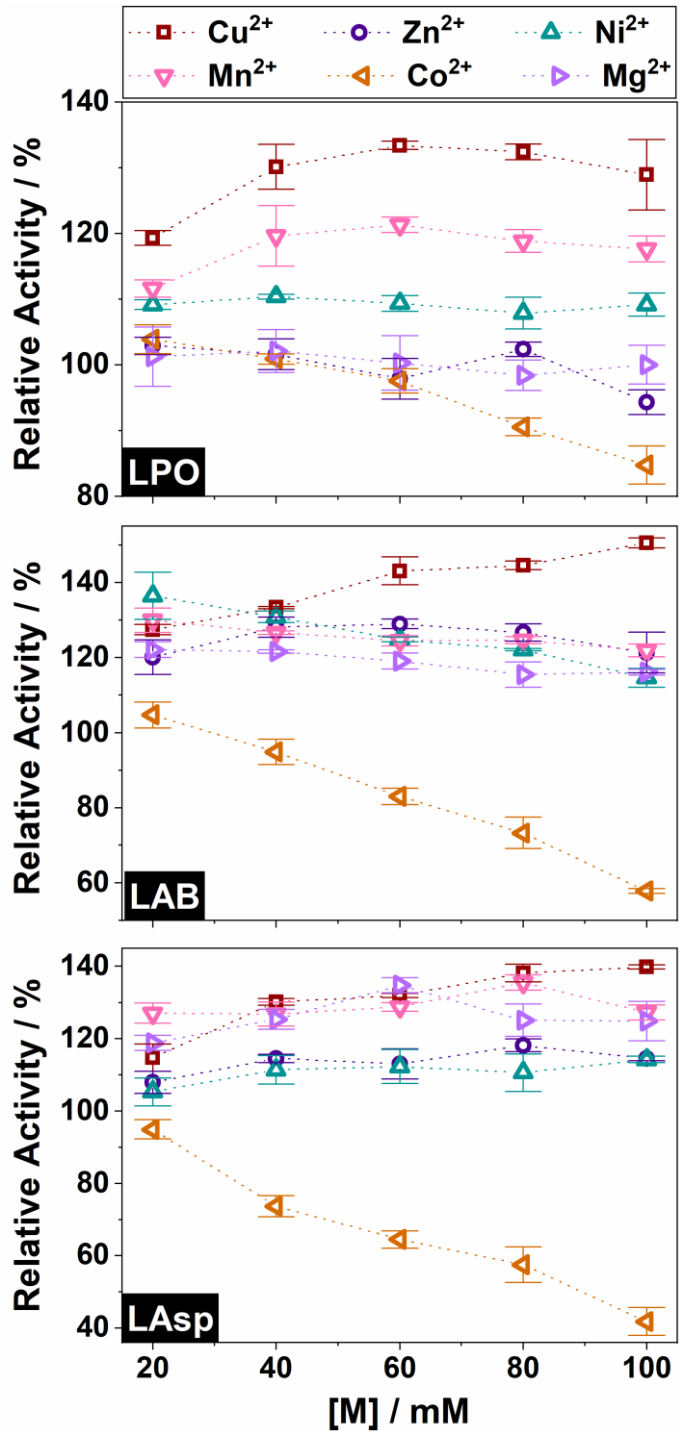

Figure 5

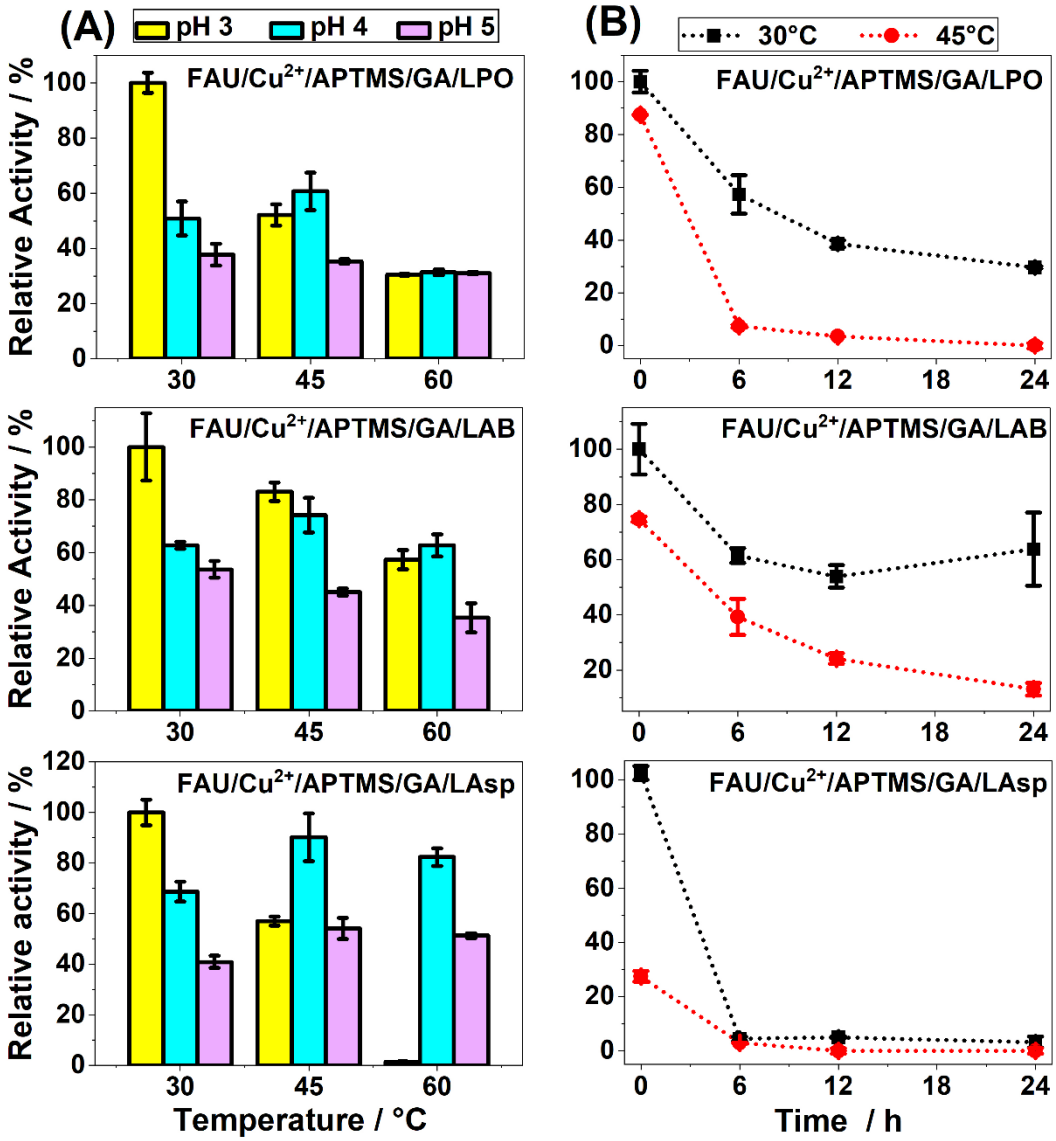
(A)
pH 3
pH 4
pH 5
FAU/Cu2+/APTMS/GA/LPO
FAU/Cu2+/APTMS/GA/LAB
FAU/Cu2+/APTMS/GA/LAsp
Relative Activity / %
Relative activity / %
Temperature / °C
(B)
30°C
45°C
Time / h

Figure 6

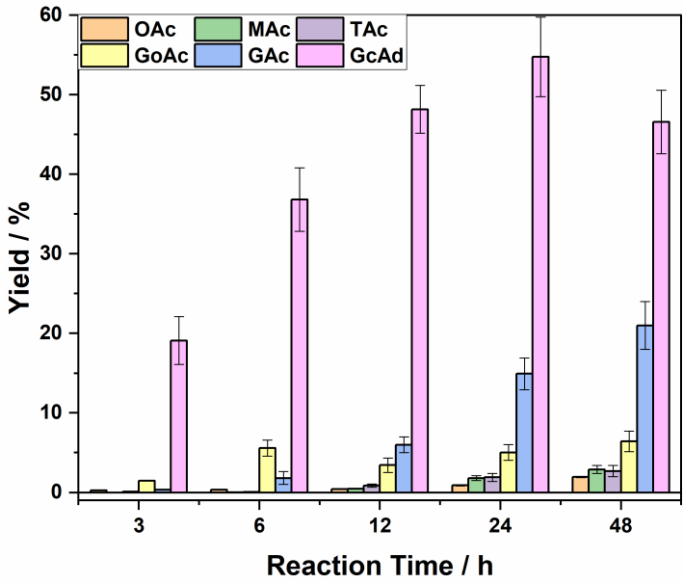
OAc
MAc
TAc
GoAc
GAc
GcAd
Yield / %
Reaction Time / h
0
10
20
30
40
50
60
3
6
12
24
48

Figure 7

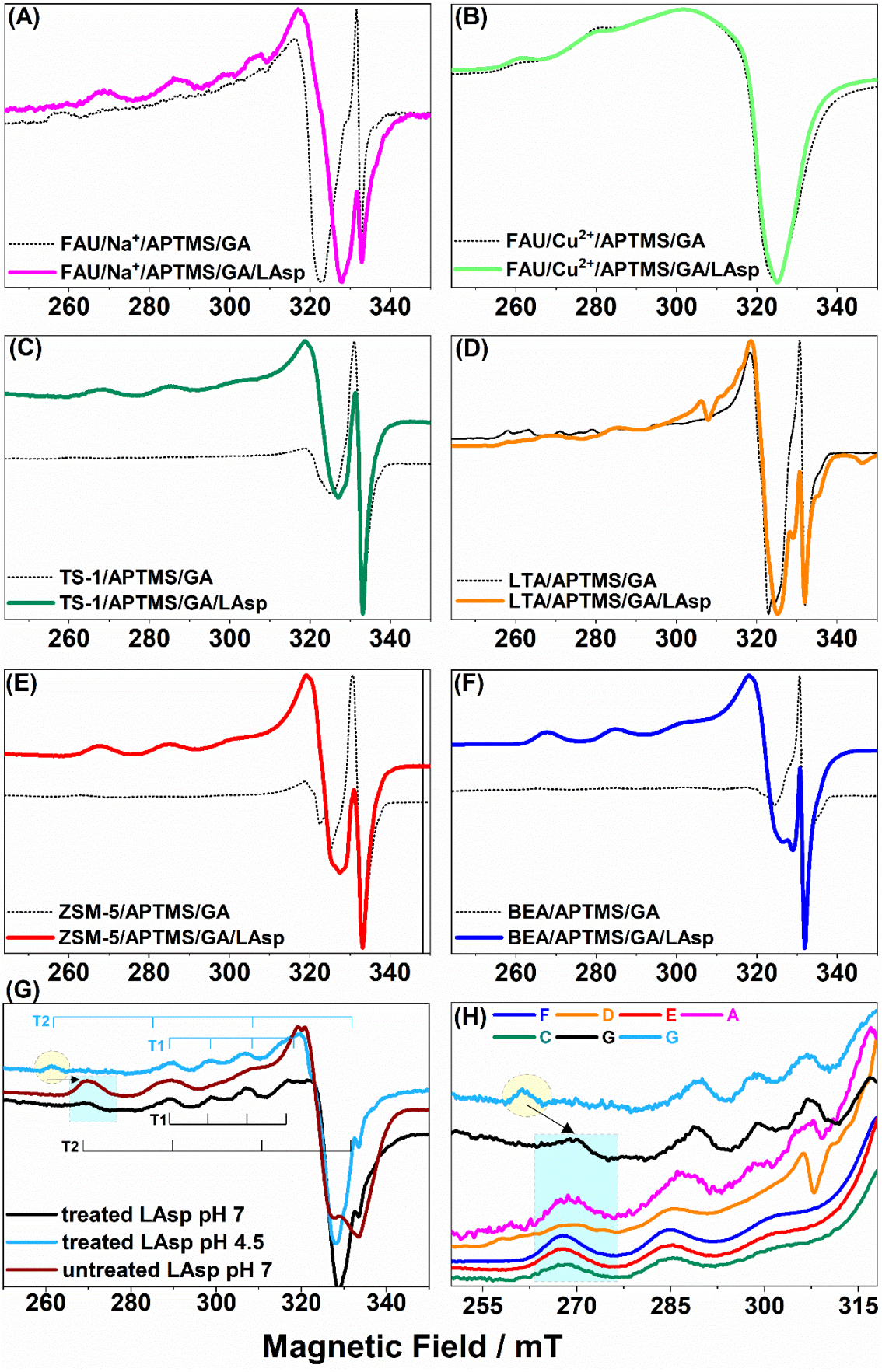
(A)
FAU/Na+/APTMS/GA
FAU/Na+/APTMS/GA/LAsp
260 280 300 320 340
(B)
FAU/Cu2+/APTMS/GA
FAU/Cu2+/APTMS/GA/LAsp
260 280 300 320 340
(C)
TS-1/APTMS/GA
TS-1/APTMS/GA/LAsp
260 280 300 320 340
(D)
LTA/APTMS/GA
LTA/APTMS/GA/LAsp
260 280 300 320 340
(E)
ZSM-5/APTMS/GA
ZSM-5/APTMS/GA/LAsp
260 280 300 320 340
(F)
BEA/APTMS/GA
BEA/APTMS/GA/LAsp
260 280 300 320 340
(G)
T2
T1
T1
T2
treated LAsp pH 7
treated LAsp pH 4.5
untreated LAsp pH 7
260 280 300 320 340
(H)
F D E A
C G G
255 270 285 300 315
Magnetic Field / mT